Supplement of Clim. Past, 21, 2465–2483, 2025 https://doi.org/10.5194/cp-21-2465-2025-supplement © Author(s) 2025. CC BY 4.0 License.





Supplement of

Mid-Holocene sea-ice dynamics and climate in the northeastern Weddell Sea inferred from an Antarctic snow petrel stomach oil deposit

Mark A. Stevenson et al.

Correspondence to: Mark A. Stevenson (mark.stevenson@arch.ox.ac.uk)

The copyright of individual parts of the supplement might differ from the article licence.

Table S1: Principal components analysis for inorganic parameters derived from XRF. Both PC 1 and PC 2 are statistically significant explaining 21% and 27% of the variance respectively. For PC 1 Al, Si, Fe, Al, Zr and Ba dominate the loadings, while for PC 2 S and Cl dominate the loadings. Bold values reflect strongest positive loadings (>0.5).

Principal component loadings	PC 1	PC 2
Al	0.668	-0.2402
Ca	-0.0205	-0.8903
Cl	-0.5118	0.5316
K	0.0386	0.1778
P	-0.8106	-0.1925
S	-0.2828	0.7355
Si	0.858	-0.0039
Br	-0.9128	-0.0927
Cu	-0.4356	-0.2622
Fe	0.6591	-0.572
Zn	-0.3456	-0.8254
Ni	-0.6025	-0.6145
Sr	-0.316	-0.804
Zr	0.5609	-0.4958
Ba	0.5727	-0.1166
Sn	-0.1935	-0.3943
Al	0.668	-0.2402
Ca	-0.0205	-0.8903

Table S2: Principal components analysis for organic parameters (bulk organics and biomarkers (TOC-normalised & ratios)). Both PC 1 and PC 2 are statistically significant explaining 30% and 24% of the variance respectively. For PC 1 $C_{18:0}/C_{18:1}$ and C:N ratio dominate the loadings (see Fig. 6 – PC 1 by time), while for PC 2 $C_{14:0}$ FA, $C_{16:0}$ FA, $C_{16:0}$ FA, $C_{18:0}$ FA and C:N dominate the loadings (see SI Fig. 6 – PC 2 by time). Bold values reflect strongest positive loadings (>0.5).

Principal component loadings	PC 1	PC 2
C _{14:0} FA	-0.2095	0.8857
C _{16:0} FA	-0.2362	0.8730
C _{16:1} FA	-0.8471	0.0396
$C_{18:0}$ FA	-0.3587	0.6929
C _{18:1} FA	-0.8623	0.0333
$C_{18:0}/C_{18:1}$ FA	0.8143	0.3042
$C_{16:0}/C_{14:0} \text{ FA}$	-0.0792	-0.0673
$C_{18:0}/C_{14:0} \text{ FA}$	-0.3177	-0.1305
% N	-0.6717	-0.6055
$\delta^{15} N$	-0.1508	0.8060
%C	0.1672	-0.1960
C:N	0.7037	0.5422
Phytol	-0.5796	-0.0284
Cholesterol	-0.6351	0.1436
Cholesterol β-epoxide	-0.5863	0.2579

Table S3: ICP-OES analysis of rock fragments adjacent to stomach oil deposit 3012MUM2. Bedrock geology of the overall Heimefrontfjella region is mainly paragneiss (Juckes, 1972).

Deposit	Mn	Si	Al	Fe	Ca	Mg	Na	Nd
3012MUM2								
(mg/kg)	237.3	503.6	25598.3	35929.4	4607.1	7877.9	857.6	48.9

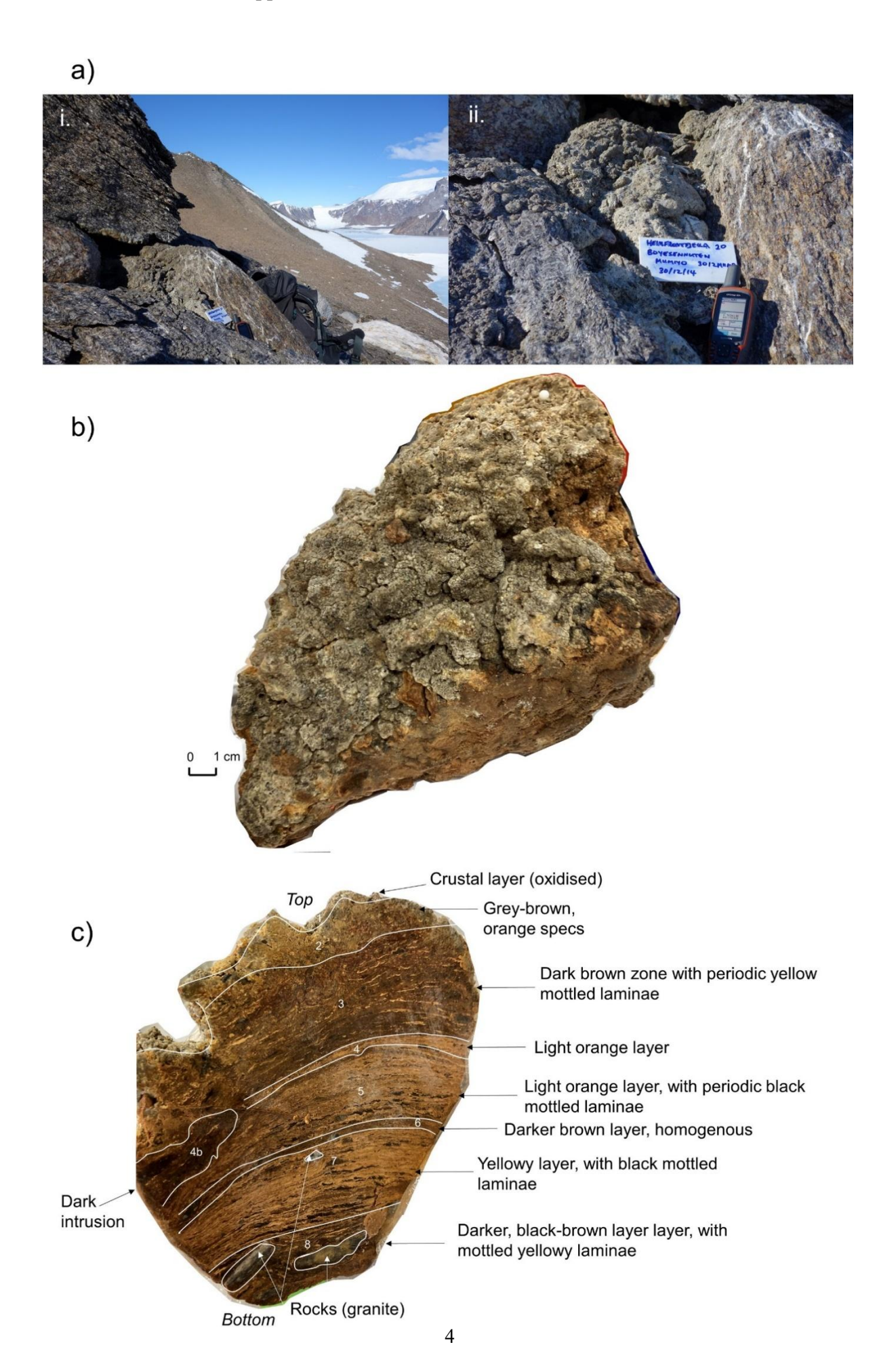


Figure S1: a) Environmental setting of the 3012MUM2 stomach oil deposit in the Heimefrontfjella Range, East Antarctica. Deposit sampled on 30.12.14 from the Boysennuten nunatak at an elevation of 1336 m.a.s.l. (coordinates: 74° 34.138 S; 11° 15.016 W). a) i. Landscape view of deposit adjacent to rock crevice nesting site; ii. Close-ups of the stomach oil deposit in situ, b) in the laboratory prior to slicing, and c) after slicing. Notations on c) indicate visual transitions between different coloured and textured layers and the presence of rocks within the deposit including: (1) an outer mamillated crustal layer with a grey hue, likely oxidised; (2) a grey-brown layer with orange specks; (3) a darker brown zone with periodic yellow mottled laminae; (4) a lighter orange layer (mostly homogeneous); (5) a light orange layer, with periodic black mottled laminae; (6) a thin homogenous darker brown layer; (7) a wide yellowy layer with black mottled laminae and a small granite rock; (8) a darker, brown-black layer with mottled yellowy laminae and two visible gneissic granite rocks. An additional dark intrusion (4b) is marked on the left of the images which was avoided during sampling.

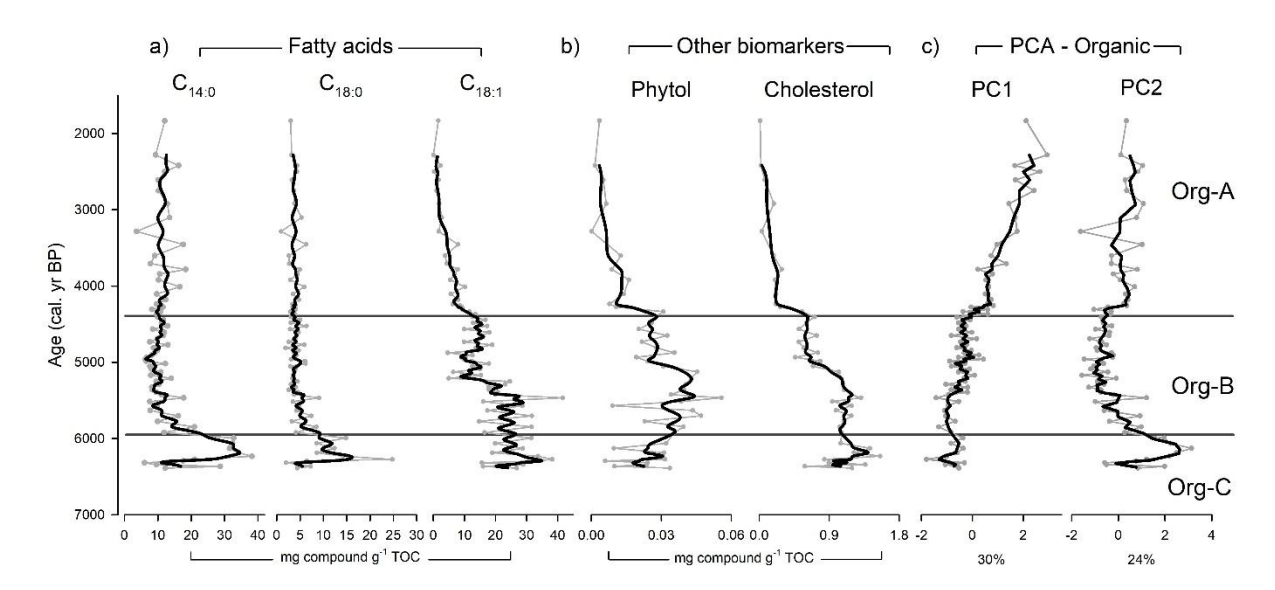


Figure S2: Organic parameters as concentrations measured in stomach oil deposit 3012MUM2, plotted the against age-depth model (Fig. 2), supplementing flux plot in Fig. 3. Smooth lines in bold are 3 point moving averages. PC1 & PC2 utilise compounds in SI Table 2. Constrained hierarchical cluster analysis was used to determine three significant clusters (Org A-C) using organic parameters in rioja (Juggins, 2020), compared with the broken-stick model (Bennett, 1996). Figure includes a) fatty acid concentrations ($C_{14:0}$, $C_{18:0}$, $C_{18:1}$); b) Other biomarkers (phytol & cholesterol).

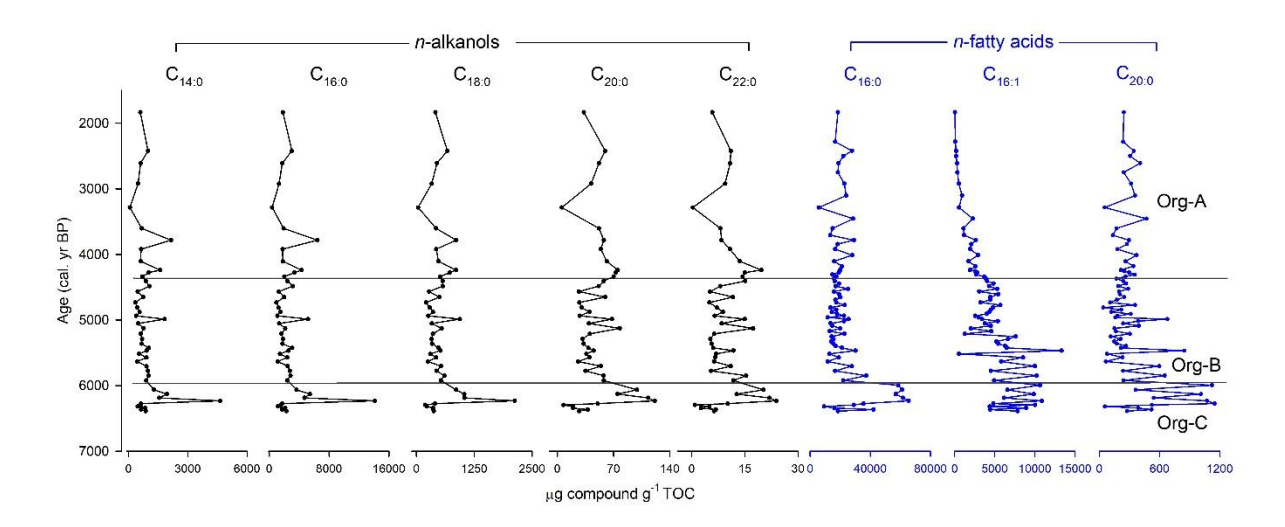


Figure S3: Concentrations of (a) key *n*-alkanols from 3012MUM2 stomach-oil deposit and (b) additional fatty acids not shown in the main paper, plotted against age-depth model from Fig. 2. Cluster boundaries uses organic parameters from Fig.3. Constrained hierarchical cluster analysis was used to determine three significant clusters (Org A-C) using only inorganic parameters (as presented in Fig. 3) in rioja (Juggins, 2020), compared with the broken-stick model (Bennett, 1996).

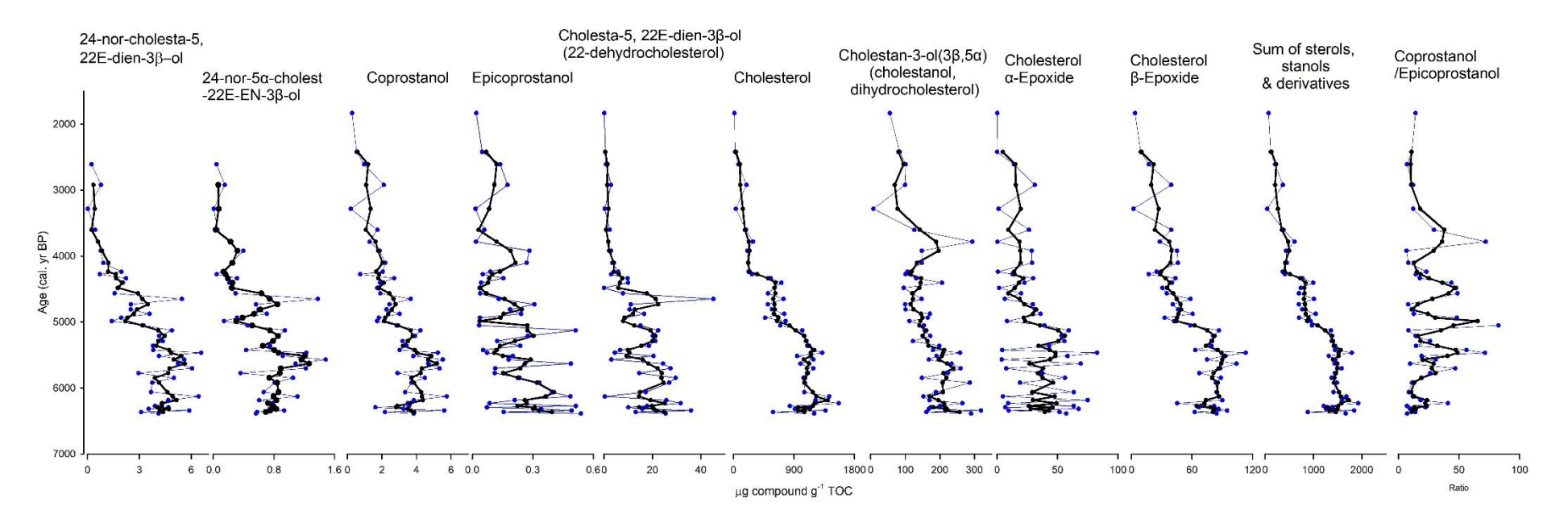


Figure S4: Full range of sterols, stanols and their derivatives identified in deposit 3012MUM2. Parameters include 24-nor-cholesta-5,22E-dien3β-ol, 24-nor-5α-cholest-22E-EN-3β-ol, coprostanol, epicoprostanol, cholesta-5, 22E-dien-3β-ol (22-dehydrocholestrol), cholesterol, cholestane-3-ol(3β,5α) (cholestanol, dehydrocholesterol), cholesterol α-Epoxide, cholesterol β-Epoxide, sum of sterols, stanols & derivatives, coprostanol/epicoprostanol. Note cholesterol and cholesterol β-epoxide utilised in PCA analysis (SI Fig. 9). Smooth lines in black bold are 3 point moving averages. Identification of cholesterol α /β-epoxide aided by Annan et al. (1993).

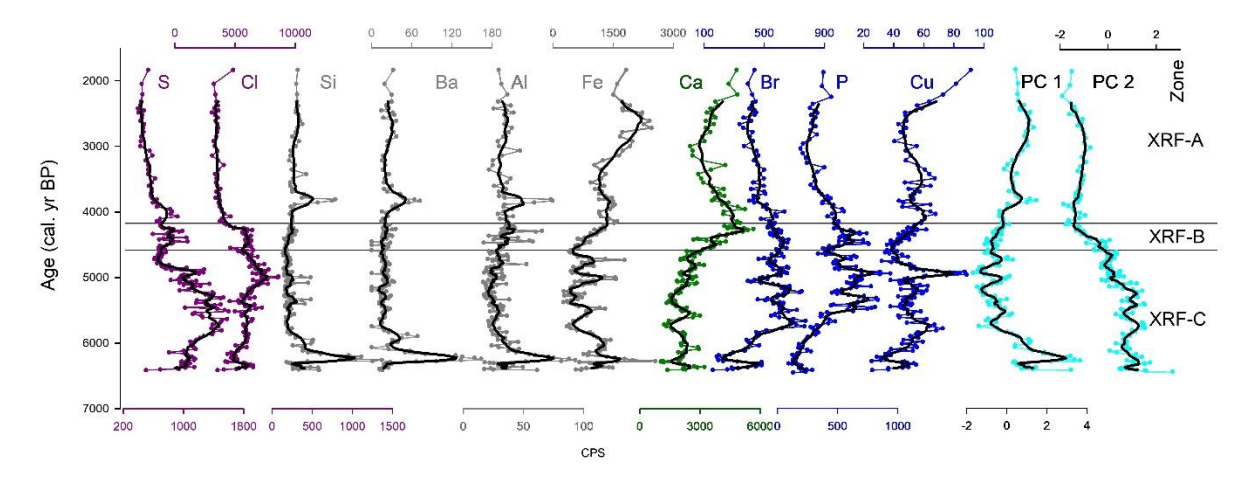


Figure S5: Key inorganic elements measured in stomach-oil deposit 3012MUM2, plotted as counts per second (CPS) against the age-depth model (Fig. 2), mirroring flux plot from Fig.4. Elements include S, Cl, Si, Ba, Al, Fe, Ca, Br, P, Cu, XRF-PC1 & XRF-PC2. Plots are coloured according to PCA groupings. Black lines indicate 7 point moving averages. Cluster boundaries (XRF-A, B & C) and XRF PCA are uniquely calculated from entire XRF dataset (also see Figure SI Fig. 6).

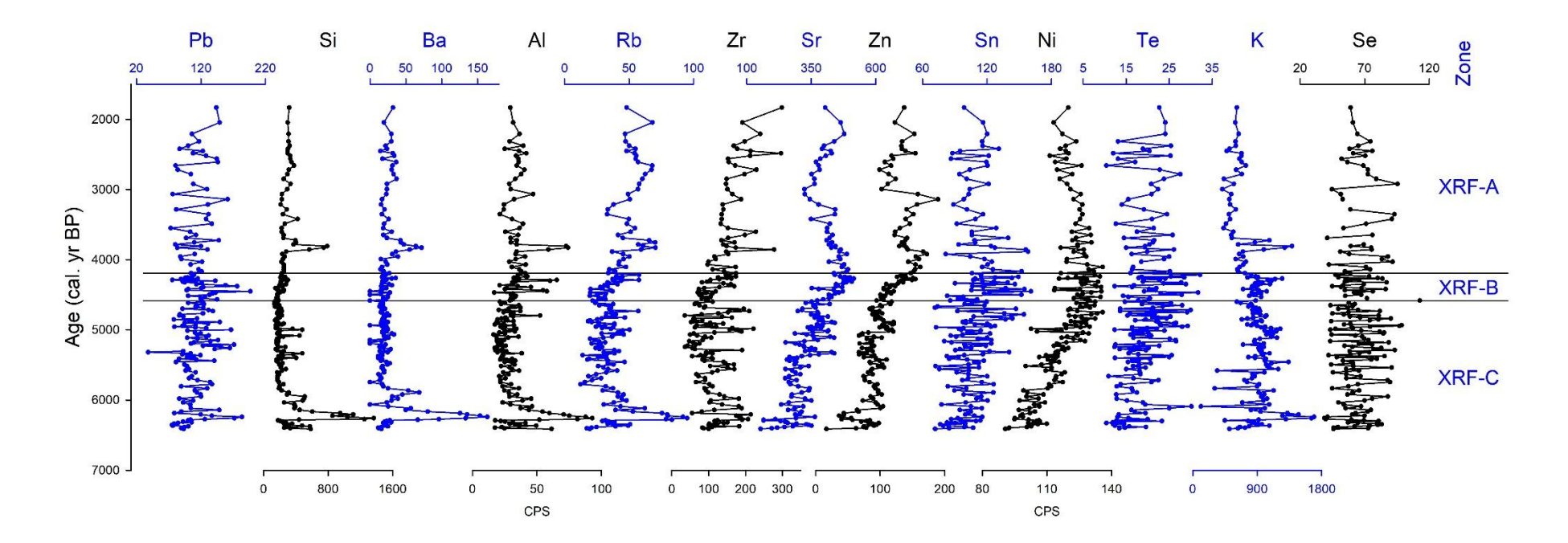


Figure S6: Selected element contributions additional to those plotted in the main paper (Pb, Si, Ba, Al, Rb, Zr, Sr, Zn, Sn, Ni, Te, K & Se) analysed by XRF core-scanning for 3012MUM2 stomach-oil deposit adjacent to XRF PCA 1 (25% variance explained), plotted against age-depth model from Fig. 2. Constrained hierarchical cluster analysis was used to determine three significant clusters (XRF A-C) using only inorganic parameters (as presented in Fig. 4) in rioja (Juggins, 2020), using the broken-stick model (Bennett, 1996).

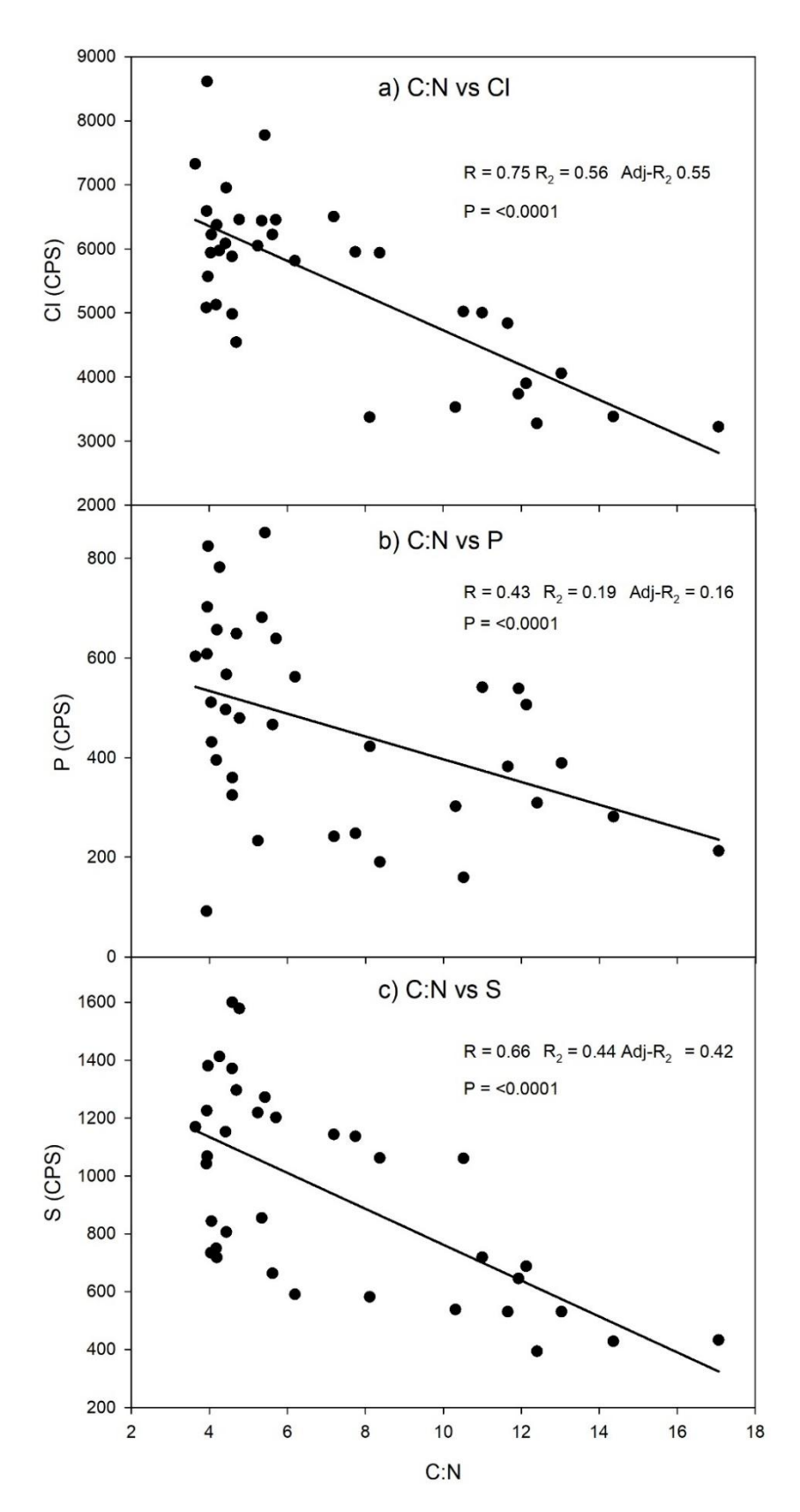


Figure S7: Negative linear relationships between C:N and (a) Cl, (b) P and (c) S. Here we show the potential role of guano as a secondary signal, in part driving some organic matter accumulation. The negative relationship is consistent with other studies (Berg et al., 2019; Hiller et al., 1988), but contrasts with a record from Marine Isotope Stage 2 (Mcclymont et al., 2022).

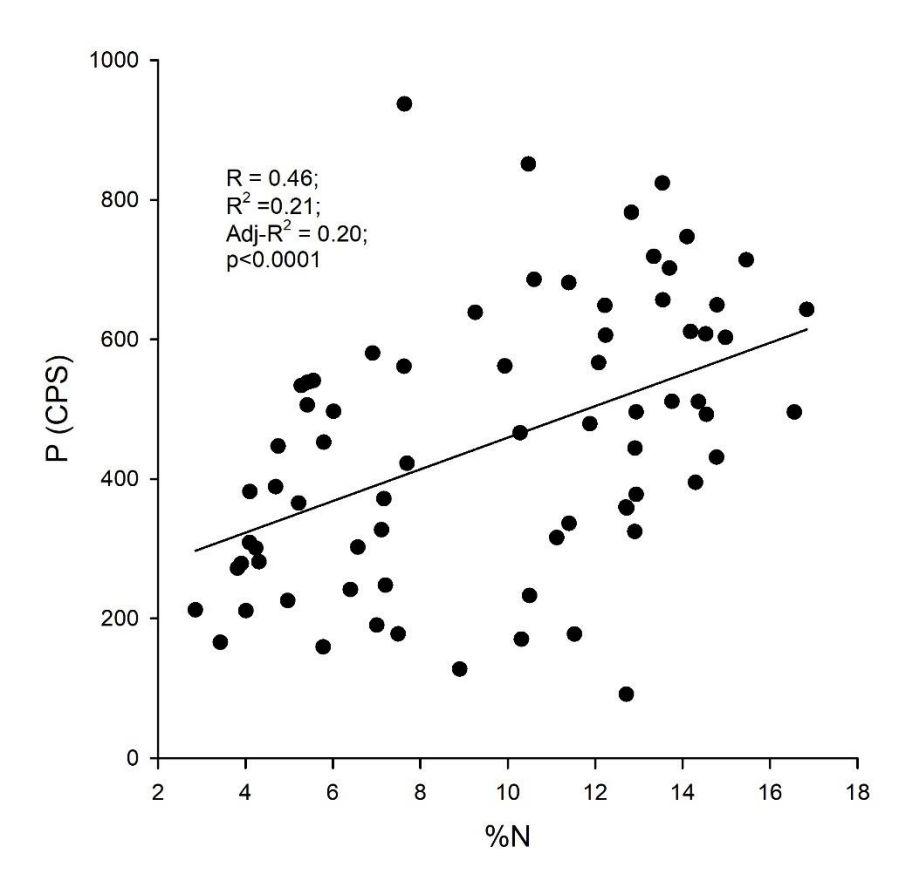


Figure S8: Positive correlation (statistically significant) between P and N in stomach oil deposit 3012MUM2 (R = 0.46; $R^2 = 0.21$; Adj- $R^2 = 0.20$; p <0.0001). As P analysed by XRF (0.1 cm) was sampled at a higher resolution than N analysed by EA (0.25 cm), P was resampled to the same resolution as N, by taking the closest value from the original XRF data point.

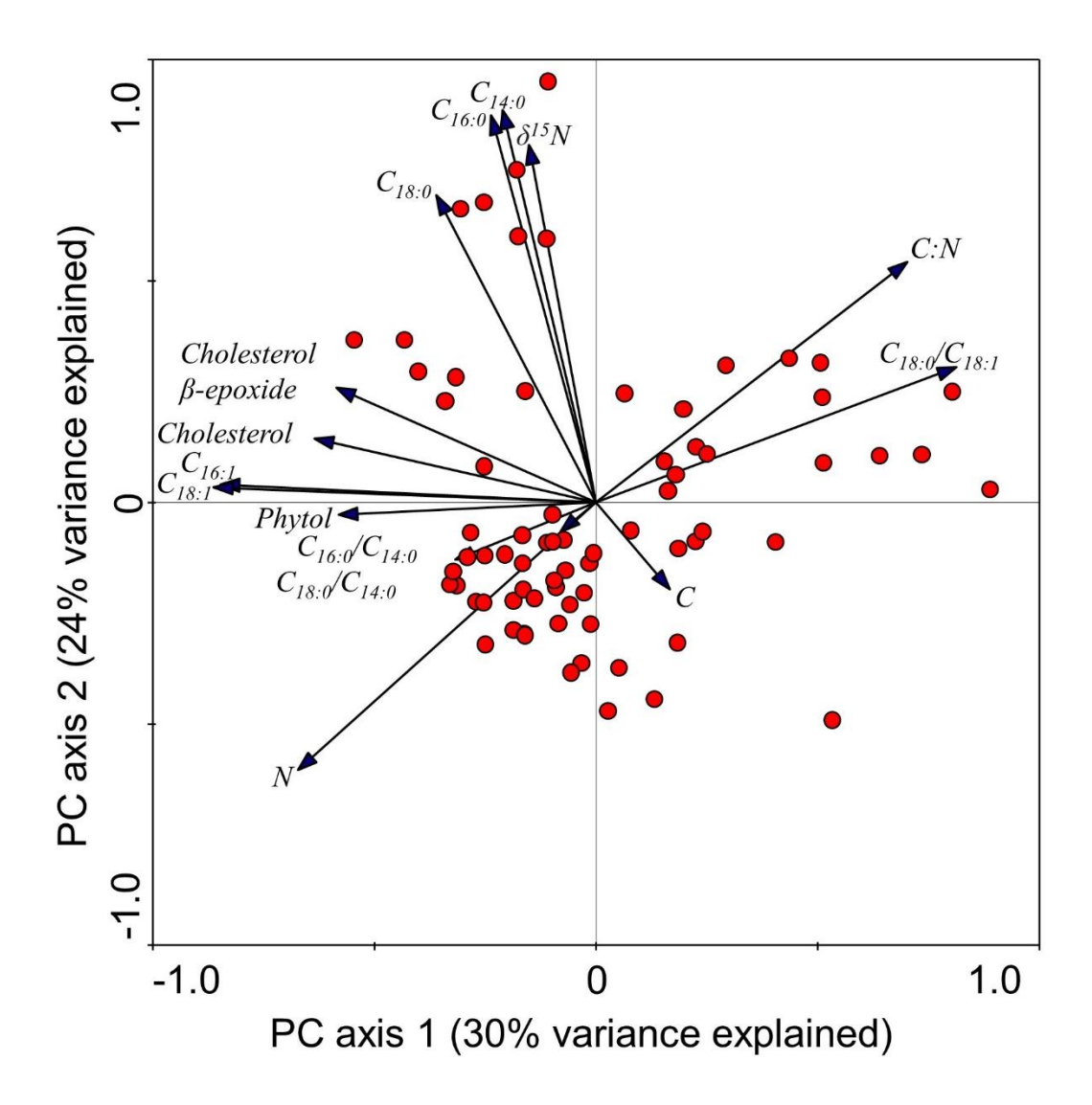


Figure S9: Principal components analysis (PC) biplot of bulk organic (C:N, C, N, δ^{15} N), lipid concentration (FA's C_{14:0}, C_{16:0}, C_{18:0}, C_{18:1}, phytol, cholesterol, cholesterol β-epoxide) and lipid ratio (C_{16:0}/C_{14:0}, C_{18:0}/C_{14:0}, C_{18:0}/C_{18:1}) based on log¹⁰ transformed and centred datasets.

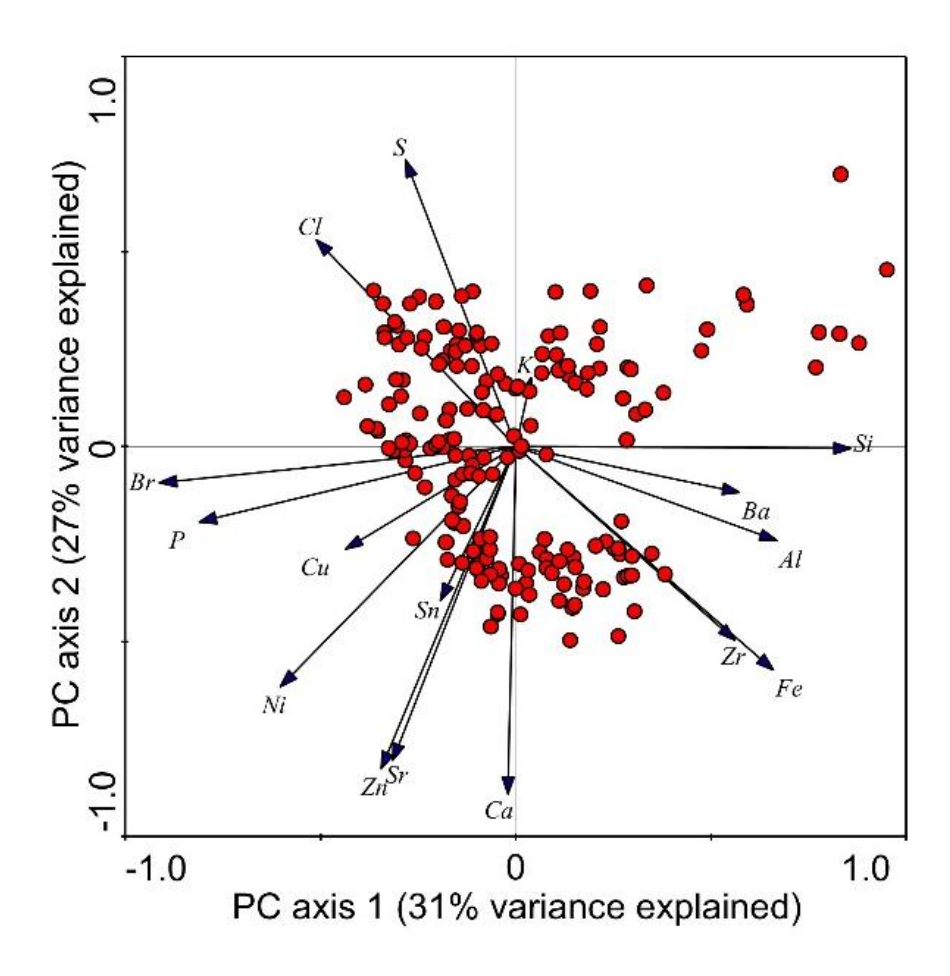


Figure S10: Principal components analysis (PC) biplot of inorganic parameters (K, Si, Ba, Al, Zr, Fe, Ca, Sr, Zn, Sn, Ni, Cu, P, Br) based on log¹⁰ transformed and centred datasets.

References

Annan, M., LeQuesne, P. W., and Vouros, P. 1993 Trimethylsilyl group migration in the mass spectra of trimethylsilyl ethers of cholesterol oxidation products. Product ion characterization by linked-scan tandem mass spectrometry *Journal of the American Society for Mass Spectrometry* 4 327-335

Bennett, K. D. 1996 Determination of the number of zones in a biostratigraphical sequence *New Phytologist* 132 155-170

Berg, S., Melles, M., Hermichen, W.-D., McClymont, E. L., Bentley, M. J., Hodgson, D. A., and Kuhn, G. 2019 Evaluation of Mumiyo Deposits From East Antarctica as Archives for the Late Quaternary Environmental and Climatic History *Geochemistry, Geophysics, Geosystems* 20 260-276

Hiller, A., Wand, U., Kämpf, H., and Stackebrandt, W. 1988 Occupation of the Antarctic continent by petrels during the past 35 000 years: Inferences from a 14C study of stomach oil deposits *Polar Biology* 9 69-77

Juckes, L. 1972: The geology of north-eastern Heimefrontfjella, Dronning Maud Land British Antarctic Survey

Juggins, S. 2020 rioja: Analysis of Quaternary Science Data. R package version 0.9-26 *University of Newcastle, Newcastle upon Tyne*

McClymont, E. L., Bentley, M. J., Hodgson, D. A., Spencer-Jones, C. L., Wardley, T., West, M. D., Croudace, I. W., Berg, S., Gröcke, D. R., Kuhn, G., Jamieson, S. S. R., Sime, L., and Phillips, R. A. 2022 Summer sea-ice variability on the Antarctic margin during the last glacial period reconstructed from snow petrel (Pagodroma nivea) stomach-oil deposits *Clim. Past* 18 381-403